



# Impact of solvents on doctor blade coatings and bathocuproine cathode interlayer for large-area organic solar cell modules

Soonil Hong<sup>a,1</sup>, Byoungwook Park<sup>a,1</sup>, Chandran Balamurugan<sup>b</sup>, Jinho Lee<sup>c,\*</sup>,  
Sooncheol Kwon<sup>b,\*\*</sup>

<sup>a</sup> Division of Advanced Materials, Korea Research Institute of Chemical Technology (KRICT), Daejeon 34114, Republic of Korea

<sup>b</sup> Department of Energy and Materials Engineering, Dongguk University-Seoul, Seoul 04620, Republic of Korea

<sup>c</sup> Department of Physics, Incheon National University, 119 Academy-ro, Incheon 22012, Republic of Korea

## ARTICLE INFO

### Keywords:

Organic solar cells  
Organic solar cell modules  
Solvent effect  
Doctor blade coating  
Bathocuproine

## ABSTRACT

Efforts to commercialize organic solar cells (OSCs) by developing roll-to-roll compatible modules have encountered challenges in optimizing printing processes to attain laboratory-level performance in fully printable OSC architectures. In this study, we present efficient OSC modules fabricated solely through printing methods. We systematically evaluated the impact of processing solvents on the morphology of crucial layers, such as the hole transport, photoactive, and electron transport layers, applied using the doctor blade coating method, with a particular focus on processability. Notably, deposition of charge transport layer using printing techniques is still a challenging task, mainly due to the hydrophobic characteristic of the organic photoactive layer. To overcome this issue, we investigated the solvent effect of a well-studied cathode interlayer, bathocuproine (BCP). We were able to form a uniform thin BCP film (~10 nm) on a non-fullerene based organic photoactive layer using the doctor bladed coating method. Our results showed that the use of volatile alcohols in the BCP processing required a delicate balance between wettability and vaporization, which contrasted with the results for spin-coated films. These findings provide important insights into improving the efficiency of printing techniques for depositing charge transport layers. The fully printed OSC modules, featuring uniform and continuous BCP layer formation, achieved an impressive power conversion efficiency of 10.8% with a total area of 10.0 cm<sup>2</sup> and a geometrical fill factor of 86.5%.

## 1. Introduction

Organic solar cells (OSCs) made from small molecules and polymers have gained attention as a promising source of renewable energy due to their low cost, lightweight, flexibility, and transparency, making them suitable for portable, wearable, and building-integrated photovoltaic applications [1–5]. Over the past few decades, researchers have made significant advancements in the development of OSCs, focusing on increasing their power conversion efficiency (PCE). These advancements include improved device structures, interfacial layers, organic photoactive materials, and other techniques, leading to a certified PCE of 18.2% in 2021 [6–10].

\* Corresponding author.

\*\* Corresponding author.

E-mail addresses: [jlee@inu.ac.kr](mailto:jlee@inu.ac.kr) (J. Lee), [kwansc12@dongguk.edu](mailto:kwansc12@dongguk.edu) (S. Kwon).

<sup>1</sup> These authors contributed equally to this work.

<https://doi.org/10.1016/j.heliyon.2023.e18209>

Received 24 February 2023; Received in revised form 6 July 2023; Accepted 11 July 2023

Available online 12 July 2023

2405-8440/© 2023 Published by Elsevier Ltd.

This is an open access article under the CC BY-NC-ND license

(<http://creativecommons.org/licenses/by-nc-nd/4.0/>).

Recently, researchers have shifted their focus to developing printed OSCs using techniques such as doctor blade coating, slot-die coating, and screen printing [11–14]. These methods are considered a step closer to large-scale production [15–21], and pioneers like Krebs and his team have explored scalable printing technologies for large-area OSCs and flexible devices using full roll-to-roll processing [22–25]. Furthermore, advancements in module structures and laser scribing pattern techniques have increased the photoactive area to total area ratio and resulted in higher module PCEs [26–28].

Despite the significant progress made in printed organic solar cells (OSCs), their reported efficiencies and performance are still lower than those of spin-coated small-area counterparts. Previous studies have mainly focused on synthesizing new photoactive materials and using time-consuming and labor-intensive testing procedures to achieve optimal device performance through spin coating. In comparison to the conventional spin coating method, where the solution is dropped onto the substrate's center and rapidly rotated to form a uniform solid film through centrifugal force, the printing method has been considered challenging for fabricating uniform films and efficient devices due to its complex coating mechanism. The printing process relies on the fluid dynamics of the meniscus, which involves the wettability and adsorption of the solution on the substrate. Therefore, controlling shear stress and substrate temperature can promote the formation of uniform and crystalline films during the relatively slow evaporation of the solution [29–32]. Although methods such as hot substrate coating, hot slot-die coating, and bilayer blade coating have shown promise, there is still limited research on the use of widely applicable high-throughput methods for fabricating large-area OSC modules [33–35]. Furthermore, despite advancements in the development of organic electron transport layers (ETLs) between the photoactive layer and top electrode, such as conjugated polyelectrolytes and small molecules, the successful printing of these interfacial layers onto hydrophobic non-fullerene-based photoactive layers has not been demonstrated [36–43]. Therefore, it is crucial to urgently demonstrate a printable OSC module prototype compatible with continuous roll-to-roll processing to facilitate the transition from laboratory to industrial scales.

In this study, we successfully prepared printed OSC modules with high power conversion efficiencies (PCEs) of 14.0% and 10.8% for active areas of 1 cm<sup>2</sup> and total areas of 10 cm<sup>2</sup>, respectively, with a geometrical fill factor of 86.5%. By investigating the relationship between printing process conditions and organic thin film morphology, we developed protocols for fabricating well-structured OSC modules using the doctor blade printing process, and analyzed the distinct effects of spin coating and meniscus processing on film morphology. Achieving a balance between wettability and solution evaporation was identified as a crucial factor in obtaining uniform surface morphology through meniscus-guided thin-film deposition. These findings indicate that efficient and scalable OSC modules can be fabricated by employing an appropriate solvent system and optimizing printing conditions.

## 2. Experimental procedures

### 2.1. Materials

Poly (3,4-ethylenedioxythiophene) polystyrene sulfonate (PEDOT:PSS), specifically Clevis P VP AI4083 from Heraeus, was diluted with isopropyl alcohol (IPA) obtained from Sigma Aldrich. The dilution was performed at volume ratios of 1:0, 1:1, and 1:2. PM6 and Y6 were purchased from 1-Material (Nano Clean Tech) and dissolved in chloroform (Sigma Aldrich) at a concentration of 12 mg/ml, using a 1:1 ratio. To this solution, PC<sub>70</sub>BM additives purchased from Nano-C were added, resulting in a concentration of 14 mg/ml. Subsequently, the photoactive solution stored at room temperature was divided into two variants, one with 0.5 vol% of 1-chloronaphthalene (CN) and one without. Bathocuproine (BCP) obtained from Sigma Aldrich was diluted to concentrations of 0.7 and 1.5 mg/ml in methanol, 1-butanol, and isopropyl alcohol (IPA) for thin and thick BCP layers. To prepare the ZnO solution, zinc acetate dihydrate and ethanolamine were dissolved in IPA and stirred for 12 h. The PTB7-Th:PC<sub>70</sub>BM solution was created by mixing PTB7-Th with PC<sub>70</sub>BM at a ratio of 1:1.8 in chlorobenzene (Sigma Aldrich). Additionally, 3 vol% of 1,8-diodooctane (Sigma Aldrich) was included to achieve a desirable concentration (13 mg/ml). Finally, the precursor solution to form MoO<sub>3</sub> was made by dissolving 5 mg of molybdenum dioxide bis(acetylacetonate) in 1 ml of a mixture of 1-butanol and cosolvent (methanol:1-butanol = 0.2:0.8).

### 2.2. Device fabrication

The Indium tin oxide (ITO)-coated glass substrates underwent a cleaning process using detergent and were subsequently ultrasonicated in deionized water, acetone, and isopropanol for 15 min each. For the fabrication of small-area normal structured OSCs, a PEDOT:PSS solution was spin-coated onto the substrates at 5000 rpm for 40 s and annealed at 150 °C for 20 min. The photoactive layer (PM6:Y6:PC<sub>70</sub>BM) was then deposited by spin coating the solution at 1200 rpm for 40 s. The BCP solutions were applied by spin coating at 5000 rpm for 20 s. In the case of large-area normal structured OSCs and OSC modules, a PEDOT:PSS solution (AI 4083 diluted in IPA) was applied using a coating blade and annealed at 150 °C for 20 min. Subsequently, the photoactive layer (PM6:Y6:PC<sub>70</sub>BM) was deposited using the doctor blade at a coating speed of 10 mm/s. The BCP solutions were also applied using the doctor blade, with the coating speed ranging from 10 mm/s to 50 mm/s. For the fabrication of large-area inverted structured OSCs, the ZnO solution was applied using a coating blade and conducted thermal treatments. The PTB7-Th:PC<sub>70</sub>BM and MoO<sub>3</sub> solutions were sequentially deposited using a coating blade. Finally, silver (Ag) was deposited onto each device through a vacuum evaporation technique conducted under vacuum condition of 1 × 10<sup>-6</sup> torr.

### 2.3. Characterization

The current density-voltage ( $J$ - $V$ ) characteristics of devices were measured using an Iviumsoft under AM1.5 illumination ( $100 \text{ mW/cm}^2$ ) with an Abet Technologies Sun 3000 under normal atmospheric conditions. The light intensity from the xenon (Xe) lamp in the solar simulator was calibrated using a National Renewable Energy Laboratory (NREL)-calibrated KG5 filtered silicon reference cell. The incident photon to current (IPCE) spectra were measured using an IPCE measurement system from PV measurements, Inc. Topographic atomic force microscopy (AFM) images were obtained using a Park System with an XE-100 microscope. For the cross-sectional images of the OSC module, transmission electron microscopy (TEM) was employed. To prepare the samples for imaging, they were first coated with sputtered carbon and platinum and then subjected to an in situ focused ion beam (FIB) process. The imaging of the samples was conducted using an FE-TEM (Tecnai F-30 S-Twin) operating at 300 kV in bright-field (BF) TEM mode.

### 3. Results and discussion

In our experiment, we utilized the doctor blade coating method, which is the most commonly used printing equipment, to prepare printed layers of organic solar cells (OSCs). The doctor blade coating method is a noncontact printing technique that involves injecting a solution between the blade and the substrate to form a meniscus. In contrast, the spin coating method applies centrifugal force. In the doctor blade process, the film forms naturally and relies on the adhesion between the bottom layer of the solution and the substrate (Fig. S1). The resulting film thickness can be theoretically derived by the concentration of the solution, the size of the gap between the blade and substrate, and the coating speed. Precise control of these parameters is essential to achieve the optimal thickness and desired surface quality with minimal morphological defects, which are crucial factors for obtaining high-performance printed OSCs. Our previous studies have shown that film morphology can be influenced by solution properties such as viscosity, boiling point, and surface energy. Hence, in this study, we focused on investigating the effect of the solvent on the doctor blade-coated photoactive layer, particularly the electron transport layer (ETL), to develop highly efficient large-area OSC modules.

OSCs typically exhibit two representative device structures: a normal type with the structure of ITO/HTL/photoactive layer/ETL/electrode, and an inverted type with the structure of ITO/ETL/photoactive layer/HTL/electrode. While both normal and inverted structures have demonstrated high efficiencies in spin-coated OSCs, most printed OSCs have been demonstrated with inverted structures due to the desirable processability of HTLs, such as molybdenum oxides, onto the hydrophobic photoactive layer through thermal evaporation. To enable the preparation of OSCs solely through printing methods, it is crucial to develop multiple layers that can be coated using printing techniques. In our case, we selected OSCs with a normal structure and without any vacuum-evaporated charge transport layers. Fig. 1a-e illustrates the doctor blade coating process for three layers (excluding the electrodes) in OSCs with a normal structure, an energy level diagram of the corresponding materials in the devices, and the molecular structures of the photoactive materials.

In the first layer, we employed the commonly used hole transport material PEDOT:PSS, which was coated to achieve the best thickness and uniformity in large-area devices. Pristine PEDOT:PSS (AI 4083) exhibited poor wetting on ITO/glass substrates and resulted in a thick film ( $\sim 100 \text{ nm}$ ) when applied at the optimal doctor blade coating speed of  $10 \text{ mm/s}$ . To improve wettability and achieve the desired thickness ( $\sim 35 \text{ nm}$ ), pristine PEDOT:PSS was diluted with an ambipolar solvent, IPA. Optical microscope (OM) images demonstrated that the diluted PEDOT:PSS solution was uniformly coated on the ITO/glass substrate using the doctor blade

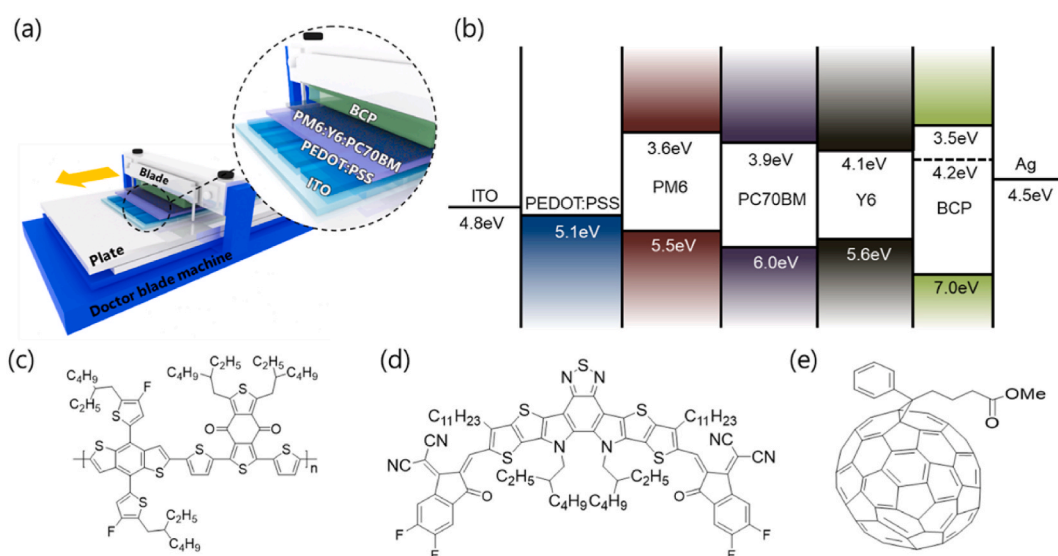


**Fig. 1.** (a) Schematic illustration of the doctor blade coating process for normal-structured OSCs. (b) Energy level diagram of the corresponding materials in devices. The molecular structures of (c) PM6, (d) Y6, and (e) PC<sub>70</sub>BM.

coating method (Fig. S2).

In the preparation of spin-coated small-area organic solar cells (OSCs), a tiny volume of a high boiling point solvent, known as a solvent additive, has been used in photoactive solutions to improve the power conversion efficiency (PCE) by 0.5%–1% [9–11]. The commonly employed solvent additives are 1,8-diiodooctane (DIO) and 1-chloronaphthalene (1-CN), which have high boiling points of 332.5 °C and 263 °C at 760 mm Hg, respectively [9–11,44,45]. While DIO has a higher boiling point and lower vapor pressure (0.0375 Pa at 25 °C) compared to 1-CN, it can oxidize in the presence of air and act as a photoacid under UV irradiation, leading to degradation of device performance. To mitigate this issue, the photoactive layers were formed using a blade coating process with the addition of 1-CN in PM6:Y6-based photoactive materials.

In terms of the spin coating method, the inclusion of 1-CN improved the morphology of the photoactive layer and resulted in slightly better phase separation, as depicted in Fig. 2a, e and (b, f), as well as Fig. S3. However, the doctor-blade-coated photoactive layer with 1-CN additive exhibited poor morphology, which had a negative impact on device performance, as shown in Fig. 2c, g and (d, h), and Fig. S4. The bulk heterojunction morphology consisted of separated donor and acceptor materials that collapsed because of the high boiling point of 1-CN, causing the doctor blade-coated photoactive layer to form under wet film conditions. This allowed sufficient time for the formation of segregated morphology. Additionally, we attempted to observe clear domains of donor and acceptor phase separation using high-resolution transmission electron microscopy (TEM). Although the TEM images did not clearly show the donor and acceptor-rich domains, they exhibited similar tendencies to the atomic force microscopy (AFM) images (Fig. S5). The natural evaporation of the solvent during the doctor blade coating process eventually acted as an additive during the spin coating, as it slowed down the rapid solvent evaporation and provided ample time for the formation of an ideal solid film. Consequently, the development of printed OSCs was carried out using a solvent additive-free photoactive layer coating.

In conventional structured OSCs, the deposition of the charge transport layer using printing techniques remains a challenge due to the hydrophobic nature of the organic photoactive layer. To address this issue, we conducted an investigation on the influence of solvents in the doctor blade coating process for a bathocuproine (BCP) organic electron transport layer (ETL), aiming to achieve a uniform thin film (~10 nm) on a nonfullerene-based organic photoactive layer. The ETL materials were dissolved in various alcohol solvents such as methanol, ethanol, 1-butanol, and IPA. These alcohol solvents possess different properties such as viscosity, surface tension, and boiling point, which directly impact the film formation on the photoactive layer.

In this study, we specifically selected three solvents: methanol (boiling point  $\approx 65$  °C), 1-butanol (boiling point  $\approx 117$  °C), and IPA (boiling point  $\approx 82.6$  °C), each possessing distinct boiling points and wettability characteristics. Methanol is commonly used for dissolving organic ETL materials due to its favorable volatility, solubility, and compatibility with the photoactive layer [40–43]. However, as depicted in Fig. 3 (a, d), the rapid evaporation of methanol is unsuitable for coating an approximately 10 nm thin film onto the organic photoactive layer based on a blade coating process. Similar to 1-butanol and IPA, the surface energy of methanol (22.7 mN/m) closely matches that of the organic photoactive layer, thereby preventing droplet formation on the substrate. At the nanometer scale, methanol evaporates before the BCP layer can fully form, resulting in circular marks on the surface of the photoactive layer. Optical microscopy (OM) images illustrate the non-uniformity of BCP film formation when employing methanol-based doctor blade coating (Fig. S6).

Fig. 3 (b, e) and (c, f) demonstrate that there is no significant difference between 1-butanol and IPA; however, a wave pattern is consistently observed when using 1-butanol in our experiments. This pattern was faintly visible under OM when BCP was coated with the high-throughput (50 mm/s) doctor blade coating process, as shown in Fig. S7. Despite 1-butanol having a slightly higher surface energy (25.0 mN/m) compared to IPA (23.3 mN/m), its excessively high boiling point causes the wet BCP film to remain on the surface

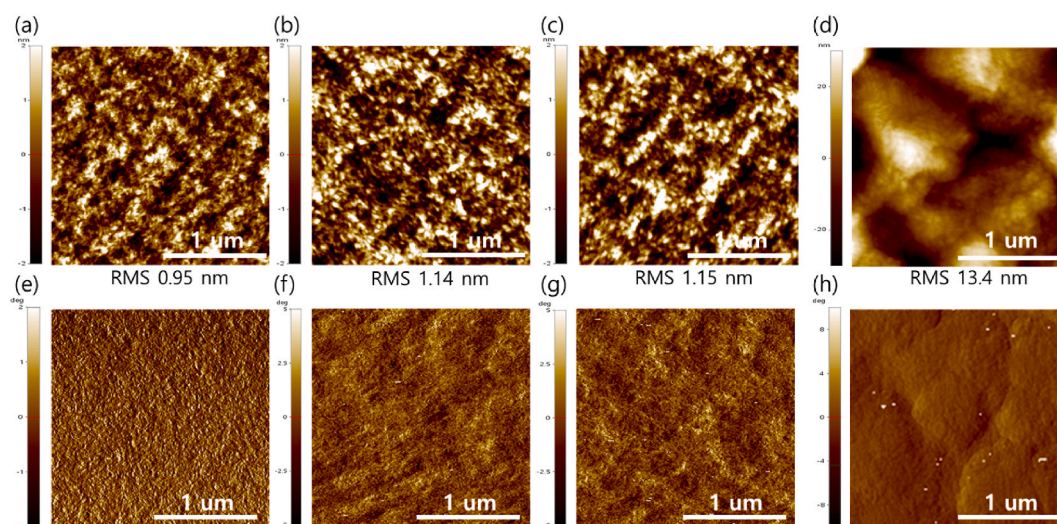


**Fig. 2.** AFM height (a–d) and phase (e–h) images of spin coated PM6:Y6:PC<sub>70</sub>BM films (a, e) without and (b, f) with CN additive, and doctor blade coated PM6:Y6:PC<sub>70</sub>BM films (c, g) without and (d, h) with CN additive.

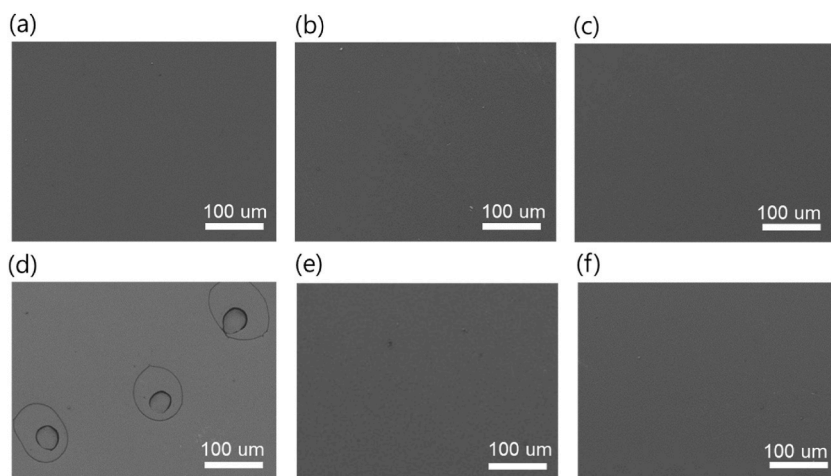


**Fig. 3.** (a) SEM images of the spin-coated BCP film with (a) methanol, (b) 1-butanol, and (c) IPA. SEM images of the doctor blade-coated BCP film with (d) ethanol, (e) 1-butanol, and (f) IPA.

of the photoactive layer for an extended period, resulting in an uneven film formation.

The  $J$ - $V$  characteristics of the spin-coated small-area and blade-coated large-area OSCs exhibited similar trends as observed in the SEM and OM images (Fig. 4a-d, and Tables 1 and 2). Due to the centrifugal forces during spin coating, the BCP ETL was uniformly coated, regardless of the solvent used. Consequently, all devices with an active area of  $4.64 \text{ mm}^2$  showed a similar PCE of approximately 15%. However, for doctor blade-coated devices with a larger active area of  $1 \text{ cm}^2$ , methanol was not suitable for BCP ETL coatings on organic photoactive layers. The use of methanol led to reduced open circuit voltage ( $V_{oc}$ ) of 0.79 V and a fill factor (FF) value of 0.51, resulting in a relatively low PCE of 10.1%. Although butanol exhibited good wettability on the organic film, the PCE was still limited to 13% due to reductions in  $V_{oc}$  and FF. The highest PCE was achieved when BCP dissolved in IPA was applied using a doctor blade. The large-area OSC demonstrated a short circuit current density ( $J_{sc}$ ) of  $24.9 \text{ mA/cm}^2$ , a  $V_{oc}$  of 0.86, an FF of 0.66, and a resulting PCE of 14.0%. The current values were similar across the different BCP solvent types, but variations were observed in  $V_{oc}$  and FF (Fig. S8). Additionally, OM images revealed that the morphology of the thick BCP layer ( $\sim 20 \text{ nm}$ ) was similar for each solvent compared to the thin BCP layer (Fig. S9). Despite the uniform thick BCP film achieved through the doctor blade coating method using IPA solvent, the insulating property of the BCP layer led to charge accumulation and ultimately resulted in lower PCEs compared to devices based on thin BCP layers (Fig. S10).

We conducted further investigations into the relationship between photovoltaic parameters and light intensity, aiming to compare the recombination characteristics among different devices [46–49]. Each photovoltaic parameter was determined based on the  $J$ - $V$  characteristics measured under varying light intensities ranging from 1 to  $100 \text{ mW/cm}^2$ . In the case of organic solar cells (OSCs), the  $J_{sc}$  values typically exhibit a power-law dependence on light intensity, which can be described as  $J_{sc} \propto I^\alpha$ , where  $I$  represents the light intensity and  $\alpha$  represents the exponential factor. When the devices exhibit weak second-order recombination, a linear relationship with  $\alpha$  approaching unity is observed, whereas a sub-linear dependence indicates strong recombination. By analyzing the linearly fitted data for OSCs, as shown in Fig. 5a, we obtained  $\alpha$  values of 0.89, 0.92, and 0.92 for methanol, 1-butanol, and IPA, respectively. The nonlinear behavior observed in devices with methanol-processed BCP ETL suggests significant nongeminate recombination losses under short-circuit conditions, indicating relatively inefficient charge collection. Additionally, the light intensity dependence of  $V_{oc}$

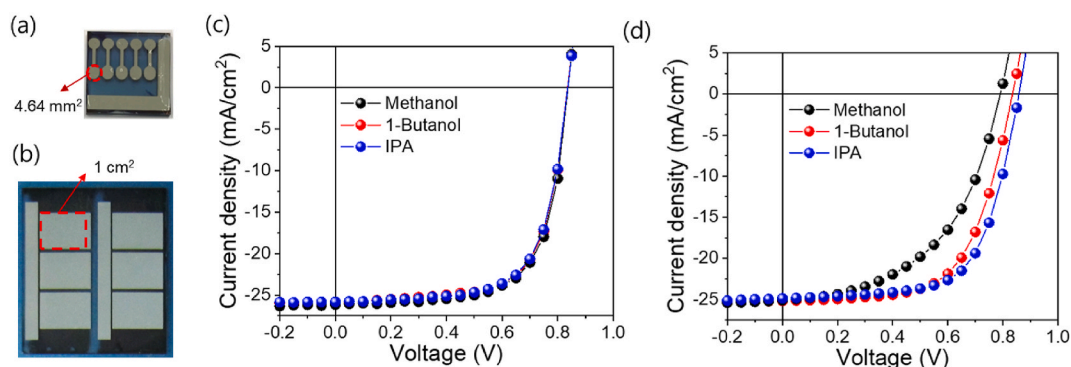


**Fig. 4.** Photographs of (a) spin-coated small-area OSCs (size:  $15 \times 15 \text{ mm}^2$ ) and (b) doctor blade-coated large-area OSCs (size:  $40 \times 46 \text{ mm}^2$ ).  $J$ - $V$  characteristics of (c) spin-coated small-area OSCs and (d) doctor blade-coated large-area OSCs for each solvent.

**Table 1**  
Photovoltaic performance parameters of the spin-coated small-area OSCs.

Area 4.64 mm <sup>2</sup>	V <sub>oc</sub> (V)	J <sub>sc</sub> (mA/cm <sup>2</sup> )	FF	PCE (%)
Methanol	0.84	26.2	0.68	14.9
1-Butanol	0.84	25.9	0.68	14.8
IPA	0.84	25.8	0.68	14.7

**Table 2**  
Photovoltaic performance parameters of the doctor blade-coated large-area OSCs.

Area 1 cm <sup>2</sup>	V <sub>oc</sub> (V)	J <sub>sc</sub> (mA/cm <sup>2</sup> )	FF	PCE (%)
Methanol	0.79	25.1	0.51	10.1
1-Butanol	0.84	25.2	0.62	13.1
IPA	0.86	24.9	0.66	14.0

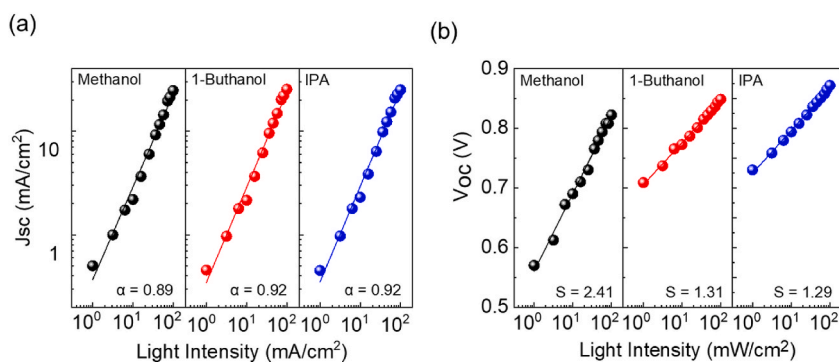


**Fig. 5.** Variation in (a) J<sub>sc</sub> and (b) V<sub>oc</sub> of OSCs as functions of light intensity.

offers insights into trap-assisted recombination during open-circuit conditions, where photogenerated charges recombine. Fig. 5b illustrates the slope of V<sub>oc</sub> versus logarithmic light intensity, where a slope greater than kT/q suggests the presence of additional trap-assisted recombination losses. For IPA, the value of 1.29 kT/q was close to unity, indicating less significant trap-assisted recombination. Conversely, when methanol was used for BCP ETL doctor blade coating, the stronger dependence of V<sub>oc</sub> on light intensity was reflected in the value of 2.41 kT/q. We speculate that the ideality factor higher than 2 might be attributed to non-uniform recombination currents within the device or tail states within the bandgap of the photoactive materials. As a result, the uniformly coated BCP ETL increased the built-in voltage across the devices due to its low work function and the suppression of recombination at interfacial trap sites, leading to the highest PCE among the printed OSCs. In the high-speed doctor blade coating (50 mm/s) of BCP ETLs, the J-V characteristics exhibited a similar trend to that observed with the low-speed doctor blade coating (10 mm/s). However, the PCE of 1-butanol-based OSCs decreased from 13.1% to 11.5%, while the IPA-based OSCs maintained a PCE of 14.0%, as shown in Fig. S11 and Table S1. This outcome can also be attributed to interfacial recombination resulting from non-uniform BCP ETL doctor blade coating (Fig. S12).

The BCP layer, serving as an organic insulator, was extremely thin. TEM images (Fig. 6a and b) confirmed that the spin coating and doctor blade coating processes uniformly coated only the photoactive and PEDOT:PSS layers. To create efficient printed large-area OSC modules, we adopted a monolithic module structure comprising four serially connected sub-cells, as depicted in Fig. 7a and b. The HTL and photoactive layer were formed without the use of an additive solvent, while the BCP ETL coating utilized the doctor blade coating method with different solvents. Among the various solvents tested in the large-area single-cell experiments, the IPA solvent-based OSC module demonstrated the highest PCE of 10.8%. This module achieved a short circuit current (I<sub>sc</sub>) of 56.0 mA, a V<sub>oc</sub> of 3.24, and an FF of 0.59 over a total area of 10 cm<sup>2</sup>, with a geometrical fill factor of 86.5% (Fig. 7c and Fig. S13) (see Table 3). However, similar to the results obtained from the large-area single cells, the module exhibited the lowest PCE of 6.57% primarily due to a reduction in V<sub>oc</sub> and FF. To assess the general solvent effect on the coating of charge transport layers on hydrophobic photoactive layers, we fabricated inverted OSCs using a doctor blade coating method with ZnO, PTB7-Th:PC<sub>70</sub>BM, and MoO<sub>3</sub> layers. Since MoO<sub>3</sub> powder is not highly soluble in IPA, methanol was added to achieve a suitable boiling point for the solution. This co-solvent system yielded improved PCEs (Fig. S14 and Table S2), highlighting the significance of solvent choice in the printing process of charge transport layers.

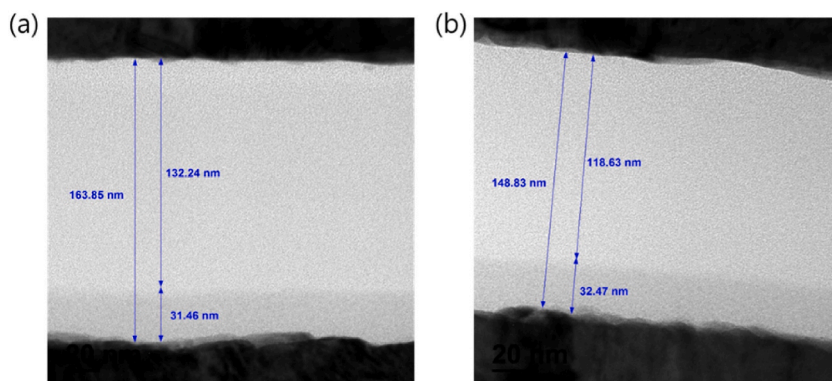


Fig. 6. TEM images of (a) spin-coated and (b) doctor blade-coated OSCs.

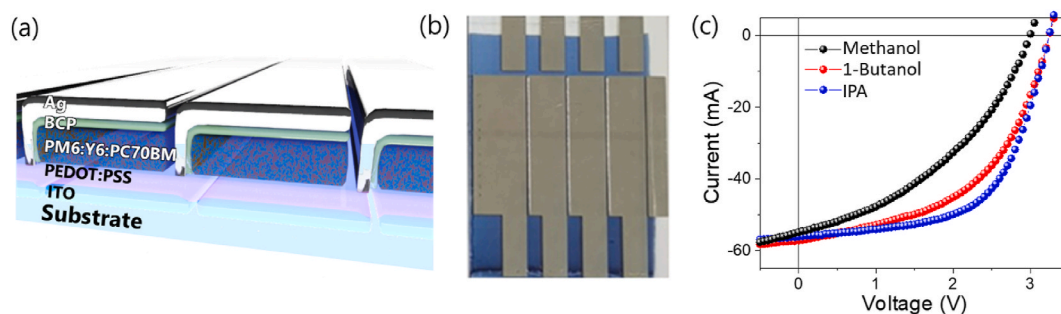


Fig. 7. (a) Schematic and (b) photographic images of the blade-coated large-area monolithic OSC modules (size  $42 \times 60 \text{ mm}^2$ ). (c) J-V characteristics of blade-coated large-area OSC modules for each solvent.

Table 3

Photovoltaic performance parameters of the doctor blade-coated large-area OSC modules.

Area $10 \text{ cm}^2$	$V_{oc}$ (V)	$I_{sc}$ (mA)	FF	APCE (%)	MPCE (%)
Methanol	3.00	54.9	0.40	7.60	6.37
1-Butanol	3.24	57.2	0.50	10.8	9.31
IPA	3.24	56.0	0.59	12.5	10.8

Geometrical fill factor 86.5%.

#### 4. Conclusions

In summary, our study successfully showcased the production of printed large-area OSC (Organic Solar Cell) modules through the optimization of processing conditions in the doctor blade coating method. Our efficient fabrication process for normally structured organic solar cells involved several steps. Firstly, we diluted the PEDOT:PSS HTL (Hole Transport Layer) solution with ambipolar IPA (Isopropyl Alcohol) solvent. Next, we prepared the non-fullerene photoactive solution without the use of any high boiling point solvent additives. We then dissolved the BCP (Bathocuproine) ETL (Electron Transport Layer) material in IPA solvent. Finally, we applied these solutions using the doctor blade coating method to create uniform films, eliminating the need for additional treatment.

Through a comprehensive analysis of the effect of the process solvent on each component layer, we discovered the significance of proper boiling point and solvent orthogonality during the coating process for the charge transport layer on the organic photoactive layer. By achieving uniform coating of the BCP ETL, we mitigated weak recombination in the interfacial region between the ETL and photoactive layer. This resulted in higher power conversion efficiencies (PCEs) in large-area printed OSCs and modules. The OSCs we produced using the doctor blade coating method achieved remarkable results, with a high PCE of 14.0% in  $1 \text{ cm}^2$  active area samples, at both low coating speeds of  $10 \text{ mm/s}$  and high coating speeds of  $50 \text{ mm/s}$ . Notably, this achievement of 14% efficiency in OSCs with a  $1 \text{ cm}^2$  area, particularly at high throughput ( $50 \text{ mm/s}$ ), is significant as it demonstrates a successful alternative to the commonly used spin coating method.

Furthermore, we expanded our demonstration to include uniform large-area OSC modules, with a total area of  $10 \text{ cm}^2$ , exhibiting the best PCE of 10.8% and a geometrical fill factor of 86.5%. These results highlight the scalability and applicability of our approach.

We believe that our findings and methodology can significantly contribute to the seamless transition of OSC technology from laboratory research to commercialization, opening up new opportunities in the field.

### Author contribution statement

Soonil Hong; Byoungwook Park: Conceived and designed the experiments; Performed the experiments.  
Chandran Balamurugan: Analyzed and interpreted the data.  
Jinho Lee; Sooncheol Kwon: Contributed reagents, materials, analysis tools or data; Wrote the paper.

### Funding statement

Dr. Soonil Hong was supported by Korea Institute of Energy Technology Evaluation and Planning (KETEP) grant funded by the Korea government (MOTIE) (No. 20223030010360 and No. 20203040010320). Dr. Byoungwook Park was supported by the Creative Materials Discovery Program through the National Research Foundation of Korea (NRF) funded by the Ministry of Science, ICT (2020M3D1A1110505). Dr. Chandran Balamurugan and Dr. Sooncheol Kwon were supported by the National Research Foundation of Korea (NRF) grant funded by the Korea government (MSIT) (No. 2021R1A2C4001904). Dr. Jinho Lee was supported by Nano-Material Technology Development Program through the National Research Foundation of Korea (NRF) funded by the Ministry of Science, ICT and Future Planning (2009-0082580).

### Data availability statement

Data included in article/supplementary material/referenced in article.

### Declaration of competing interest

The authors declare that they have no known competing financial interests or personal relationships that could have appeared to influence the work reported in this paper.

### Acknowledgments

This work was partly supported by Korea Institute of Energy Technology Evaluation and Planning (KETEP) grant funded by the Korea government (MOTIE) (No. 20223030010360 and No. 20203040010320). This work was also supported by the National Research Foundation of Korea (NRF) grant funded by the Korea government (MSIT) (No. 2021R1A2C4001904), and Nano-Material Technology Development Program through the National Research Foundation of Korea funded by the Ministry of Science, ICT and Future Planning (2009-0082580), and the Creative Materials Discovery Program through the National Research Foundation of Korea (NRF) funded by the Ministry of Science, ICT (2020M3D1A1110505).

### Appendix A. Supplementary data

Supplementary data to this article can be found online at <https://doi.org/10.1016/j.heliyon.2023.e18209>.

### References

- [1] M. Riede, D. Spoltore, K. Leo, Organic solar cells—the path to commercial success, *Adv. Energy Mater.* 11 (2021), 2002653.
- [2] K. Fukuda, K. Yu, T. Someya, The future of flexible organic solar cells, *Adv. Energy Mater.* 10 (2020), 2000765.
- [3] Z. Hu, J. Wang, X. Ma, J. Gao, C. Xu, K. Yang, Z. Wang, J. Zhang, F. Zhang, A critical review on semitransparent organic solar cells, *Nano Energy* 78 (2020), 105376.
- [4] D. Wang, H. Liu, Y. Li, G. Zhou, L. Zhan, H. Zhu, X. Lu, H. Chen, C.-Z. Li, High-performance and eco-friendly semitransparent organic solar cells for greenhouse applications, *Joule* 5 (2021) 945–957.
- [5] H. Yao, J. Hou, Recent advances in single-junction organic solar cells, *Angew. Chem.* 134 (2022), e202209021.
- [6] M. Green, E. Dunlop, J. Hohl-Ebinger, M. Yoshita, N. Kopidakis, X. Hao, Solar cell efficiency tables (version 57), *Prog. Photovoltaics Res. Appl.* 29 (2021) 3–15.
- [7] H. Hoppe, N.S. Sariciftci, Organic solar cells: an overview, *J. Mater. Res.* 19 (2004) 1924–1945.
- [8] Z. Zheng, J. Wang, P. Bi, J. Ren, Y. Wang, Y. Yang, X. Liu, S. Zhang, J. Hou, Tandem organic solar cell with 20.2% efficiency, *Joule* 6 (2022) 171–184.
- [9] X. Xu, Y. Li, Q. Peng, Ternary blend organic solar cells: understanding the morphology from recent progress, *Adv. Mater.* 34 (2022), 2107476.
- [10] S. Kwon, H. Kang, J.-H. Lee, J. Lee, S. Hong, H. Kim, K. Lee, Effect of processing additives on organic photovoltaics: recent progress and future prospects, *Adv. Energy Mater.* 7 (2017), 1601496.
- [11] J. Yuan, Y. Zhang, L. Zhou, G. Zhang, H.-L. Yip, T.-K. Lau, X. Lu, C. Zhu, H. Peng, P.A. Johnson, M. Leclerc, Y. Cao, J. Ulanski, Y. Li, Y. Zou, Single-junction organic solar cell with over 15% efficiency using fused-ring acceptor with electron-deficient core, *Joule* 3 (2019) 1–12.
- [12] Q. Liu, Y. Jiang, K. Jin, J. Qin, J. Xu, W. Li, J. Xiong, J. Liu, Z. Xiao, K. Sun, S. Yang, X. Zhang, L. Ding, 18% Efficiency organic solar cells, *Sci. Bull.* 65 (2020) 272–275.
- [13] L. Zhu, M. Zhang, W. Zhong, S. Leng, G. Zhou, Y. Zou, X. Su, H. Ding, P. Gu, F. Liu, Y. Zhang, Progress and prospects of the morphology of non-fullerene acceptor based high-efficiency organic solar cells, *Energy Environ. Sci.* 14 (2021) 4341–4357.

- [14] D. Luo, W. Jang, D.D. Babu, M.S. Kim, D.H. Wang, A.K.K. Kyaw, Recent progress in organic solar cells based on non-fullerene acceptors: materials to devices, *J. Mater. Chem.* 10 (2022) 3255–3295.
- [15] P. Xue, P. Cheng, R.P.S. Han, X. Zhan, Printing fabrication of large-area non-fullerene organic solar cells, *Mater. Horiz.* 9 (2022) 194–219.
- [16] G. Ji, W. Zhao, J. Wei, L. Yan, Y. Han, Q. Luo, S. Yang, J. Hou, C.-Q. Ma, 12.88% efficiency in doctor-blade coated organic solar cells through optimizing the surface morphology of a ZnO cathode buffer layer, *J. Mater. Chem.* 7 (2019) 212–220.
- [17] M. Yi, S. Hong, J.-R. Kim, H. Kang, J. Lee, K. Yu, S. Kee, W. Lee, K. Lee, Modification of a PEDOT:PSS hole transport layer for printed polymer solar cells, *Sol. Energy Mater. Sol. Cells* 153 (2016) 117–123.
- [18] Y. Mao, C. Guo, D. Li, W. Li, B. Du, M. Chen, Y. Wang, D. Liu, T. Wang, Molecular ordering and performance of ternary nonfullerene organic solar cells via bar-coating in air with an efficiency over 13, *ACS Appl. Mater. Interfaces* 11 (2019) 35827–35834.
- [19] J. Wei, C. Zhang, G. Jia, Y. Han, I. Ismail, H. Li, Q. Luo, J. Yang, C.-Q. Ma, Roll-to-roll printed stable and thickness-independent ZnO:PEI composite electron transport layer for inverted organic solar cells, *Sol. Energy* 193 (2019) 102–110.
- [20] S. Ganesan, S. Mehta, D. Gupta, Fully printed organic solar cells – a review of techniques, challenges and their solutions, *Opto-electron. Rev.* 27 (2019) 298–320.
- [21] D. Corzo, K. Almasabi, E. Bihar, S. Macphee, D. Rosas-Villalva, N. Gasparini, S. Inal, D. Baran, Digital inkjet printing of high-efficiency large-area nonfullerene organic solar cells, *Adv. Mater. Technol.* 4 (2019), 1900040.
- [22] F.C. Krebs, T. Tromholt, M. Jørgensen, Upscaling of polymer solar cell fabrication using full roll-to-roll processing, *Nanoscale* 2 (2010) 873–886.
- [23] R. Søndergaard, M. Hösel, D. Angmo, T.T. Larsen-Olsen, F.C. Krebs, Roll-to-roll fabrication of polymer solar cells, *Mater. Today Off.* 15 (2012) 36–49.
- [24] F.C. Krebs, N. Espinosa, M. Hösel, R.R. Søndergaard, M. Jørgensen, 25th Anniversary article: rise to power – OPV-based solar parks, *Adv. Mater.* 26 (2014) 29–39.
- [25] J.E. Carlé, M. Helgesen, O. Hagemann, M. Hösel, I.M. Heckler, E. Bundgaard, S.A. Gevorgyan, R.R. Søndergaard, M. Jørgensen, R. García-Valverde, S. Chaouki-Almagro, J.A. Villarejo, F.C. Krebs, Overcoming the scaling lag for polymer solar cells, *Joule* 1 (2017) 274–289.
- [26] L. Lucera, F. Machui, P. Kubis, H.D. Schmidt, J. Adams, S. Strohm, T. Ahmad, K. Forberich, H.-J. Egelhaaf, C.J. Brabec, Highly efficient, large area, roll coated flexible and rigid OPV modules with geometric fill factors up to 98.5% processed with commercially available materials, *Energy Environ. Sci.* 9 (2016) 89–94.
- [27] S. Hong, H. Kang, G. Kim, S. Lee, S. Kim, J.-H. Lee, J. Lee, M. Yi, J. Kim, H. Back, J.-R. Kim, K. Lee, A series connection architecture for large-area organic photovoltaic modules with a 7.5% module efficiency, *Nat. Commun.* 7 (2016), 10279.
- [28] R. Sun, Q. Wu, J. Guo, T. Wang, Y. Wu, B. Qiu, Z. Luo, W. Yang, Z. Hu, J. Guo, M. Shi, C. Yang, F. Huang, Y. Li, J. Min, A layer-by-layer architecture for printable organic solar cells overcoming the scaling lag of module efficiency, *Joule* 4 (2020) 1–13.
- [29] J. Yuan, D. Liu, H. Zhao, B. Lin, X. Zhou, H.B. Naveed, C. Zhao, K. Zhou, Z. Tang, F. Chen, W. Ma, Patterned blade coating strategy enables the enhanced device reproducibility and optimized morphology of organic solar cells, *Adv. Energy Mater.* 11 (2021), 2100098.
- [30] Y. Li, L. Deng, G. Du, Y. Li, X. Zhao, W. Deng, Additive-free organic solar cells with enhanced efficiency enabled by unidirectional printing flow of high shear rate, *Org. Electron.* 97 (2021), 106274.
- [31] F. Aziz, A.F. Ismail, Spray coating methods for polymer solar cells fabrication: a review, *Mater. Sci. Semicond. Process.* 39 (2015) 416–425.
- [32] S. Hong, J. Lee, H. Kang, K. Lee, Slot-die coating parameters of the low-viscosity bulk-heterojunction materials used for polymer solar cells, *Sol. Energy Mater. Sol. Cells* 112 (2013) 27–35.
- [33] N. Al-Shekailli, S. Hashim, F.F. Muhammadsharif, K. Sulaiman, M.Z. Al-Abri, Efficiency and stability improvement of organic solar cells based on PTB7:PCBM through hot-substrate coating, *J. Electron. Mater.* 50 (2021) 6828–6835.
- [34] S. Song, K.T. Lee, C.W. Koh, H. Shin, M. Gao, H.Y. Woo, D. Vak, J.Y. Kim, Hot slot die coating for additive-free fabrication of high performance roll-to-roll processed polymer solar cells, *Energy Environ. Sci.* 11 (2018) 3248–3255.
- [35] S. Dong, K. Zhang, B. Xie, J. Xiao, H.-L. Yip, H. Yan, F. Huang, Y. Cao, High-performance large-area organic solar cells enabled by sequential bilayer processing via nonhalogenated solvents, *Adv. Energy Mater.* 9 (2019), 1802832.
- [36] D. Zhou, W. You, F. Yang, R. Chen, H. Xu, Y. Tong, B. Hu, L. Hu, Y. Xie, L. Chen, N-type self-doped hyperbranched conjugated polyelectrolyte as electron transport layer for efficient nonfullerene organic solar cells, *ACS Appl. Mater. Interfaces* 13 (2021) 50187–50196.
- [37] D. Zhou a, Y. Li, H. Zhang, H. Zheng, X. Shen, W. You, L. Hu, L. Han, Y. Tong, L. Chen, N-type small molecule electron transport materials with D-A-D conjugated core for non-fullerene organic solar cells, *Chem. Eng. J.* 452 (2023), 139260.
- [38] D. Zhou, S. Xiong, L. Chen, X. Cheng, H. Xu, Y. Zhou, F. Liu, Y. Chen, A green route to a novel hyperbranched electrolyte interlayer for nonfullerene polymer solar cells with over 11% efficiency, *Chem. Commun.* 54 (2018) 563–566.
- [39] D. Zhou, X. Cheng, H. Xu, H. Yang, H. Liu, F. Wu, L. Chen, Y. Chen, Interface-induced face-on orientation of the active layer by self-assembled diblock conjugated polyelectrolytes for efficient organic photovoltaic cells, *J. Mater. Chem.* 4 (2016) 18478–18489.
- [40] C. Feng, X. Wang, Z. He, Y. Cao, Formation mechanism of PFN dipole interlayer in organic solar cells, *Sol. RRL* 5 (2021), 2000753.
- [41] Z.-G. Zhang, B. Qi, Z. Jin, D. Chi, Z. Qi, Y. Li, J. Wang, Perylene diimides: a thickness-insensitive cathode interlayer for high performance polymer solar cells, *Energy Environ. Sci.* 7 (2014) 1966–1973.
- [42] F. Jafari, B.R. Patil, F. Mohtaram, A.L.F. Cauduro, H.-G. Rubahn, A. Behjat, M. Madsen, Inverted organic solar cells with non-clustering bathocuproine (BCP) cathode interlayers obtained by fullerene doping, *Sci. Rep.* 9 (2019), 10422.
- [43] C.-C. Chang, C.-F. Lin, J.-M. Chiou, T.-H. Ho, Y. Tai, J.-H. Lee, Y.-F. Chen, J.-K. Wang, L.-C. Chen, K.-H. Chen, Effects of cathode buffer layers on the efficiency of bulk-heterojunction solar cells, *Appl. Phys. Lett.* 96 (2010), 263506.
- [44] S. Lee, J. Kong, K. Lee, Air-stable organic solar cells using an iodine-free solvent additive, *Adv. Energy Mater.* 6 (2016), 1600970.
- [45] C. McDowell, M. Abdelsamie, M.F. Toney, G.C. Bazan, Solvent additives: key morphology-directing agents for solution-processed organic solar cells, *Adv. Mater.* 30 (2018), 1707114.
- [46] L.J.A. Koster, M. Kemerink, M.M. Wien, K. Maturová, R.A.J. Janssen, Quantifying bimolecular recombination losses in organic bulk heterojunction solar cells, *Adv. Mater.* 23 (2011) 1670–1674.
- [47] A.K.K. Kyaw, D.H. Wang, V. Gupta, W.L. Leong, L. Ke, G.C. Bazan, A.J. Heeger, Intensity dependence of current–voltage characteristics and recombination in high-efficiency solution-processed small-molecule solar cells, *ACS Nano* 7 (2013) 4569–4577.
- [48] Z. Liu, S. Niu, N. Wang, Light illumination intensity dependence of current-voltage characteristics in polymer solar cells with solution-processed titanium chelate as electron extraction layer, *Sol. Energy* 155 (2017) 1044–1051.
- [49] K.D. Rosenthal, M.P. Hughes, B.R. Luginbuhl, N.A. Ran, A. Karki, S.-J. Ko, H. Hu, M. Wang, H. Ade, T.-Q. Nguyen, Quantifying and understanding voltage losses due to nonradiative recombination in bulk heterojunction organic solar cells with low energetic offsets, *Adv. Energy Mater.* 9 (2019), 1901077.